

## Wide frequencies range of spin excitations in a rare-earth Bi-doped iron garnet with a giant Faraday rotation

Sergii Parchenko, Andrzej Stupakiewicz, Isao Yoshimine, Takuya Satoh, and Andrzej Maziewski

Citation: [Applied Physics Letters](#) **103**, 172402 (2013); doi: 10.1063/1.4826248

View online: <http://dx.doi.org/10.1063/1.4826248>

View Table of Contents: <http://scitation.aip.org/content/aip/journal/apl/103/17?ver=pdfcov>

Published by the [AIP Publishing](#)

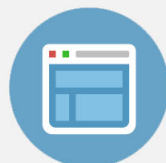
---

### Advertisement:



## Re-register for Table of Content Alerts

Create a profile.



Sign up today!



# Wide frequencies range of spin excitations in a rare-earth Bi-doped iron garnet with a giant Faraday rotation

Sergii Parchenko,<sup>1</sup> Andrzej Stupakiewicz,<sup>1,a)</sup> Isao Yoshimine,<sup>2</sup> Takuya Satoh,<sup>2,3</sup> and Andrzej Maziewski<sup>1</sup>

<sup>1</sup>Laboratory of Magnetism, Faculty of Physics, University of Białystok, Białystok 15-424, Poland

<sup>2</sup>Institute of Industrial Science, The University of Tokyo, Tokyo 153-8505, Japan

<sup>3</sup>PRESTO, Japan Science and Technology Agency, Tokyo 102-0076, Japan

(Received 8 July 2013; accepted 6 October 2013; published online 22 October 2013)

Ultrafast magnetization dynamics of a rare-earth Bi-doped garnet were studied using an optical pump-probe technique via the inverse Faraday effect. We observed a wide range of frequency modes of the magnetization precession, covering two orders of magnitude. The excitation efficiency of low-frequency precessions in the GHz range, together with a significant beating effect, strongly depended on the amplitude of the external magnetic field. On the contrary, high-frequency precession was independent of the external magnetic field. The obtained results may be exploited in the development of wide class of microwave and magneto-optical devices.

© 2013 AIP Publishing LLC. [<http://dx.doi.org/10.1063/1.4826248>]

Recent research has revealed the fascinating role of electron-spin-based phenomena in spintronic and magnonic devices operating in a wide frequency range. Optical non-contact methods offer special ways of studying local spin-density effects with high spatial and temporal resolution. On the other hand, switching of the magnetization in magnetic materials with the help of femtosecond laser pulses is of great interest for magnetic information storage/processing. The switching speed has been extended to the picosecond time-scale, as has been demonstrated in a GdFeCo alloy.<sup>1</sup> In such multisublattice materials, the switching is a result of a demagnetization process due to an exchange interaction using a circularly polarized laser pulse. Non-thermal optical coherent control and magnetization switching have been observed in ferrimagnetic garnet systems via photomagnetism<sup>2,3</sup> and the inverse Faraday effect (IFE).<sup>4</sup> Spatially shaped control of spin wave propagation by light pulses via the IFE has also been reported in rare-earth Bi-doped iron garnet (BIG).<sup>5</sup> Recently, spin-wave excitations and spin-current effects in garnet-based structures have been demonstrated.<sup>6,7</sup> Garnet films are used in magnonic crystals,<sup>8</sup> where both the Gilbert damping parameter and the precession frequency of spin waves are determined by magnetic dipole interactions. High-quality garnet films offer the opportunity of constructing devices with large functional properties. Technology for fabricating garnet at thicknesses from micro- to nano-scales can provide an extremely wide variety of compositions. By using rare-earth ion substitution at dodecahedral sites in the garnet matrix, it is possible to vary the refractive index, the Faraday rotation, optical absorption, magnetic properties, and so on.<sup>9,10</sup> Generally, garnets are perfect materials for a broad class of magneto-optical devices, including components for optical communication in the near-infrared (NIR) wavelength region, high-frequency switchers, and microwave filters.<sup>11-13</sup>

In this Letter, we report the findings from our study of a rare-earth BIG single crystal with a giant Faraday rotation of

up to 40°. We observed non-thermal magnetization dynamic excitation using circularly polarized femtosecond pulses via the IFE. We measured the amplitude and precession frequency as functions of the external magnetic field and the polarization of pump light. We observed magnetization precession with distinct frequencies in the form of a field-independent high-frequency mode at about 410 GHz and a field-dependent low-frequency mode in the range of 2–12 GHz. For the low-frequency range, we observed a beating process, which was the result of exciting spatially distributed magnetostatic spin waves. We have clarified the origin of the beating observed in the experiment by comparing with the numerical calculations.

In our experiments, we used a Gd<sub>4/3</sub>Yb<sub>2/3</sub>BiFe<sub>5</sub>O<sub>12</sub> single crystal, grown by a liquid phase epitaxial method, with (111) plane orientation and a thickness of 380 μm. At room temperature, the saturation magnetization,  $M_S$ , was 90 G, the magnetic anisotropy constant,  $H_U$ , was 620 Oe, and the Curie temperature,  $T_C$ , was 573 K. Gilbert damping,  $\alpha$ , of 0.02 has been measured in a similar material using ferromagnetic (FM) resonance.<sup>5</sup>

To observe the ultrafast spin dynamics of the sample under femtosecond laser pulse excitation, we carried out time-resolved measurements in a transmission geometry at room temperature using a magneto-optical pump-probe method. Pump pulses with a duration of about 100 fs from a Ti:sapphire laser system with an amplifier and optical parametric oscillator (Spectra-Physics) at a 500 Hz repetition rate and a wavelength of 1400 nm were directed at an angle of incidence of about 10° from the sample normal, while probe pulses with a wavelength of 800 nm were incident perpendicular to the sample. The pump beam was focused to a spot of about 100 μm in diameter, giving a fluence of about 45 mJ/cm<sup>2</sup>. The probe beam spot size was about two times smaller. The probe to pump intensity ratio was about 1:100. The delay time  $\Delta t$  between the pump and the probe pulses could be adjusted to up to 2 ns (Fig. 1). The polarization of the pump light was tuned in a wide range by using a Berek compensator. A magnetic field,  $H_{||}$ , generated by an

<sup>a)</sup> Author to whom correspondence should be addressed. Electronic mail: and@uwb.edu.pl. FAX: +48 85 745 7223.

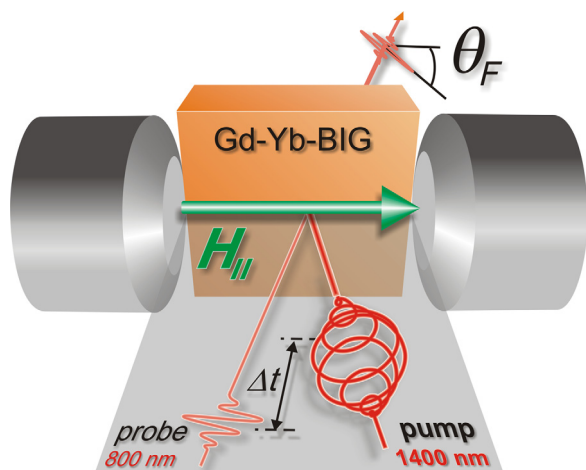


FIG. 1. Schematic illustration of the sample and experimental setup.

electromagnet, was applied parallel to the sample plane. The maximum amplitude of the magnetic field was 4.35 kOe. We measured the perpendicular component of the magnetization,  $m_z$ , representing the Faraday rotation angle,  $\theta_F$ , of the probe pulses, as a function of the delay time,  $\Delta t$ . We also studied the magnetization reversal process in a static regime at room temperature in a transmission geometry by using the Faraday effect in a wavelength range of 750–850 nm and external magnetic field,  $H_\perp$ , perpendicular to the sample surface. To detect the Faraday rotation  $\theta_F$  (see inset in Fig. 2), we used a lock-in amplifier with a standard modulation technique.

Generally, the Faraday rotation in rare-earth garnets with Bi impurities has a strong dependence on the NIR wavelength. Usually, enhanced Faraday rotation is accompanied by a large absorption.<sup>10</sup> In particular, giant Faraday rotation is caused by an increase of the spin-orbit splitting in the excited states due to the formation of hybrid molecular orbits between the 3d orbital in  $\text{Fe}^{3+}$  and the 2p orbital in  $\text{O}^{2-}$ , mixed with the 6p orbital in  $\text{Bi}^{3+}$ , which has a large spin-orbit interaction parameter.<sup>14</sup> We measured the Faraday rotation in a static regime near the 800 nm transmittance peak (inset in Fig. 2) typical of rare-earth garnets, caused by the 4f-5s electron transition.<sup>15</sup> Figure 2 shows hysteresis

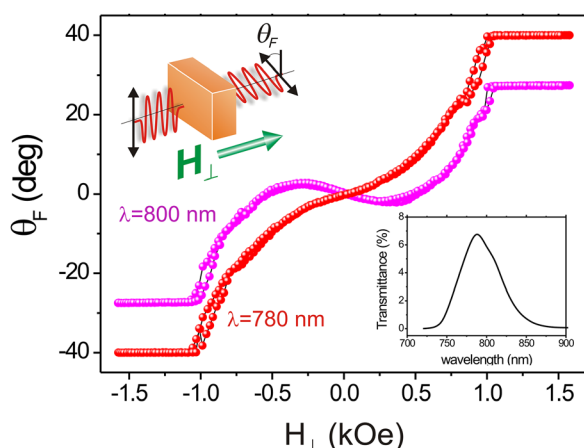


FIG. 2. Hysteresis loops measured as Faraday rotation for different wavelengths. Insets show the Faraday geometry and the transmittance dependence near a wavelength of 800 nm.

loops observed in the sample at wavelengths of 780 nm and 800 nm. The sample exhibited magnetization reversal without coercivity and had a giant Faraday rotation of up to 40° when saturated in the perpendicular direction with  $H_\perp$  of about 1 kOe. The shape of the loops was dependent on the wavelength, confirming the different and opposite contributions to the magnetic signal from the rare earth and iron sublattices at temperatures above the compensation point.<sup>10</sup> The reason for the sign inversion of the Faraday rotation is reorientation of sublattices magnetization, respectively, to direction of external magnetic field.<sup>16</sup>

Multisublattice systems with rare earth and transition metals are very promising for ultrafast magnetization switching on picosecond timescales<sup>17</sup> and spin wave excitation with pulsed light irradiation.<sup>5</sup> Generally, the magnetism in the rare earth element originates from 4f localized electrons, in contrast to Fe, where the magnetic properties occur due to the 3d delocalized conduction electrons. The rare earth ion sublattice is polarized by the Fe sublattice and becomes magnetically oriented antiparallel due to an exchange interaction. We measured the ultrafast dynamics of magnetization in the rare-earth BIG crystal as functions of the polarization of the pump light and the external in-plane magnetic field,  $H_\parallel$ . Figure 3 shows the magnetization precession (Faraday rotation angle  $\theta_F$ ) for left-handed,  $\sigma^+$  and right-handed,  $\sigma^-$ , circularly polarized laser pulses with  $H_\parallel = 1.2$  kOe. The maximum rotation angle was high, at about 4°. We observed two scales of the delay time,  $\Delta t$ , where the behavior differed, one at up to 30 ps and a much longer one in the 0.1–1.6 ns range. The dependence of the long-delay oscillation amplitude as a function of the pump polarization is shown in the inset in Fig. 3. For linear polarization of the pump light, the magnetization precession vanished. However, magnetization precessions with opposite phases were triggered by  $\sigma^+$  and  $\sigma^-$  polarizations, as a non-thermal characteristic of the ultrafast dynamics. This is consistent with an optically induced effective magnetic field along the perpendicular direction to the sample plane during femtosecond laser pulse excitation in a garnet via the inverse Faraday effect.<sup>4</sup> The magnetization vector in this case precesses around the effective magnetic field as a result of the action of different contributions:

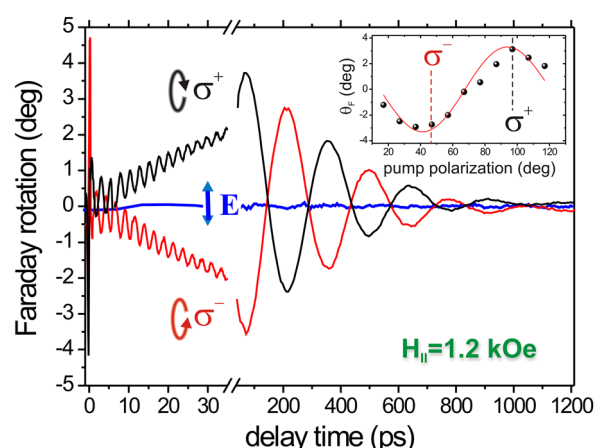


FIG. 3. Time-resolved Faraday rotation in different time scales for circular and linear polarizations of the pump laser pulses. Inset shows polarization dependence of magnetization precession amplitude.

the external in-plane magnetic field, the photoinduced effective field, and the magnetic anisotropy field.

At the initial  $\Delta t$ , a Faraday rotation transient representing precessional motion of the magnetization vector with a frequency of about 410 GHz was observed. We observed clear opposite phase precession of the high-frequency mode. Fig. 4(a) shows precession dependencies for different magnetic field amplitudes. During about 60 ps, we observed simultaneous relaxation of the high-frequency precession and excitation of the low-frequency precession of the magnetization. This dynamic behavior within a short time scale may be the result of exchange resonance<sup>18</sup> between magnetic ions in the garnet sublattices. These results confirm that a high-frequency precession at 410 GHz is practically, independent of the external magnetic field (see inset in Fig. 4(a)), with pump light in a wide spectral range of 800–1600 nm.

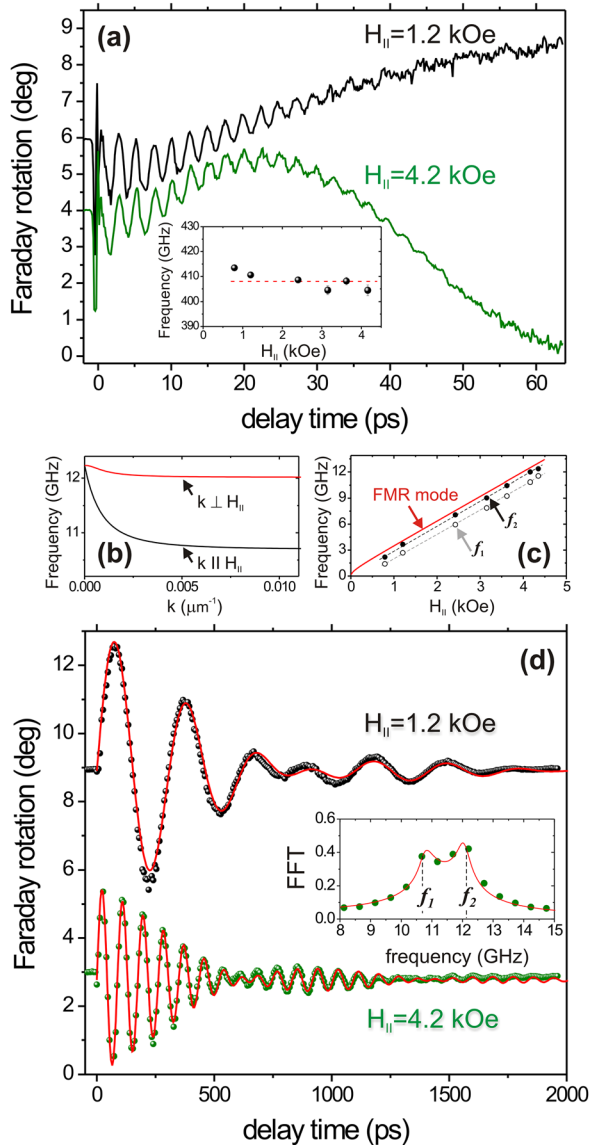


FIG. 4. Time-resolved Faraday rotation as a function of the delay time,  $\Delta t$ , for different amplitudes of  $H_{\parallel}$  in two time scales: (a) up to 60 ps and (d) up to 2 ns. Frequency as a function of magnetic field amplitude,  $H_{\parallel}$ , for (inset in (a)) high-frequency and (c) low-frequency modes. The dispersion curves for  $H_{\parallel} = 4.2$  kOe (b). The red solid lines in Fig. 4(d) and the FFT spectrum in the inset are the results of numerical calculation using Eq. (1) for  $H_{\parallel} = 4.2$  kOe.

Similar results have been observed in LuIG films with an exchange resonance mode at about 650 GHz at room temperature.<sup>19</sup> Generally, the exchange resonance frequency can be tuned by modifying the impurity concentration, exchange constants, magnetization, etc. In the rare-earth BIG sample at room temperature, the exchange field between the Fe and rare-earth sublattices is much weaker than that between the octahedral and tetrahedral iron sublattices. In the case of the magnetic rare-earth impurity in our garnet crystal, the magnitude of the saturation magnetization is determined by the tetrahedral ( $M_d$ ), octahedral ( $M_a$ ), and dodecahedral ( $M_c$ ) sublattices<sup>10</sup> and is given by  $M_S = M_d - M_a - M_c$ . In our case, the exchange resonance frequency can be determined mainly by a magnetization that is less than that in pure garnet or LuIG. Thus, we obtained a smaller value of the exchange frequency compared with that in LuIG.<sup>19</sup> In addition, Figure 4(a) shows that, for  $H_{\parallel} = 4.2$  kOe, the low-frequency mode precession was modulated by a higher-frequency oscillation.

The next part of this paper is focused on analysis of the low-frequency precession mode. We performed a Fast Fourier transform (FFT) to obtain the power spectrum and confirmed the presence of different oscillation frequencies (see inset in Fig. 4(d)). In our sample, with low Gilbert damping, the excitation of propagating spin waves led to a magnetic field-dependent frequency of the precession dynamics (see Fig. 4(d)). This appears as additional peaks in the frequency spectrum of the dynamics.<sup>20</sup> Spin wave excitation in a 380  $\mu\text{m}$ -thick garnet crystal can induce a spatial distribution of the magnetization orientation within the spot of the probe beam, thus, leading to a mixed precession with broadened frequencies, and exhibiting a damping-beating precession process. Such a beating mode has been observed in LuIG films.<sup>21</sup> In our sample, two clear modes with frequencies  $f_1$  and  $f_2$  appeared at  $H_{\parallel} = 4.2$  kOe (see inset in Fig. 4(d)). The lower and higher frequency components  $f_1$  and  $f_2$  come from the backward volume magnetostatic waves (BVMSWs) with wavevectors  $\mathbf{k}$  parallel and perpendicular to the external magnetic field  $H_{\parallel}$ , respectively. Figure 4(b) shows the frequency dispersions  $f(\mathbf{k})$  with the lowest order of BVMSWs for  $H_{\parallel} = 4.2$  kOe. Note that the BVMSW can exist even with  $\mathbf{k}$  perpendicular to  $H_{\parallel}$  in the presence of the out-of-plane magnetic anisotropy.<sup>22</sup> Thus, in the case of our sample, the spin dynamics can be described as Faraday rotation transients using the following damped harmonic function:<sup>5</sup>

$$\theta_F(\Delta t) = A \int d\vec{k} h(\vec{k}) \sin(\vec{k} \cdot \vec{r} - 2\pi f(\vec{k})\Delta t) \exp(-2\alpha\pi f(\vec{k})\Delta t), \quad (1)$$

where  $A$  is the amplitude and  $h(\mathbf{k})$  is the Fourier transform of the spatial intensity distribution of the pump spot. The results of numerical calculations using Eq. (1) were in good agreement with the experimental points and FFT spectrum (see Fig. 4(d)). Figure 4(c) plots both frequencies  $f_1$  and  $f_2$  obtained from the experimental data for different values of  $H_{\parallel}$ . The solid line in this figure was determined by the FM mode using the Kittel formula with  $H_U = 620$  Oe and  $M_S = 90$  Gs. The measured frequencies  $f_1$  and  $f_2$  were lower than the FM mode frequencies, which is consistent with



Fig. 4(b). We have previously confirmed BVMSW excitation in a garnet sample with a thickness of  $110\text{ }\mu\text{m}$ .<sup>5</sup> Thus, in our sample, we observed different types of spin precession with different frequencies: (i) high-frequency precession at about 410 GHz, in the form of an exchange resonance mode, (ii) a frequency-modulated signal in the range  $\Delta t < 100\text{ ps}$  with high- and low-frequency modes, and (iii) mainly two low-frequency field-dependent precessions in the 2–12 GHz range due to a beating process as a result of contributions from the two BVMSW modes.

In summary, we investigated non-thermal optically excited spin precession via the IFE in a rare-earth BIG single crystal with a large Faraday rotation. We observed that different frequency modes of the spin precession in the GHz and sub-THz ranges strongly depended on the polarization of the pump laser pulses. The high-frequency mode with the field-independent precession could be related to an exchange resonance mode between magnetic sublattices in the sample. Under an external in-plane magnetic field, we observed magnetization precession with low-frequency modes as a superposition of spatially distributed spin waves. We observed a beating process resulting from the summation of two low-frequency contributions, which have recently been found to be related to observed BVMSW modes in similar materials. The experimental results and numerical calculations were in good agreement. In addition, these modes were modulated by a high-frequency mode that was observed with a delay time up to about 50 ps.

A wide frequency range of spin precession and large spatial propagation variations may be useful for wavenumber, magnetic resonance, and dispersion control, not to mention offering options for tuning the ultrafast dynamic response with a giant Faraday rotation. The results of our investigations demonstrate the importance of developing microwave and magneto-optical isolators for a wide class of physical phenomena in photonics, spintronics, and magnonics, and will be particularly important in enabling such materials to be incorporated directly with metal or semiconductor systems for evaluating opto-magnonic technologies.

The authors thank S. Demokritov for fruitful discussions. This work was supported by the Foundation for Polish Science Team Programme co-financed by the EU European Regional Development Fund, OPIE 2007-2013.

- <sup>1</sup>A. Kirilyuk, A. V. Kimel, and Th. Rasing, *Rev. Mod. Phys.* **82**, 2731 (2010).
- <sup>2</sup>F. Atoneche, A. M. Kalashnikova, A. V. Kimel, A. Stupakiewicz, A. Maziewski, A. Kirilyuk, and T. Rasing, *Phys. Rev. B* **81**, 214440 (2010).
- <sup>3</sup>A. Stupakiewicz, M. Pashkevich, A. Maziewski, A. Stognij, and N. Novitskii, *Appl. Phys. Lett.* **101**, 262406 (2012).
- <sup>4</sup>F. Hansteen, A. Kimel, A. Kirilyuk, and Th. Rasing, *Phys. Rev. B* **73**, 014421 (2006).
- <sup>5</sup>T. Satoh, Y. Terui, R. Moriya, B. A. Ivanov, K. Ando, E. Saitoh, T. Shimura, and K. Kuroda, *Nature Photon.* **6**, 662 (2012).
- <sup>6</sup>H. Kurebayashi, O. Dzyapko, V. E. Demidov, D. Fang, A. J. Ferguson, and S. O. Demokritov, *Nature Mater.* **10**, 660 (2011).
- <sup>7</sup>Y. Kajiwara, K. Harii, S. Takahashi, J. Ohe, K. Uchida, M. Mizuguchi, H. Umezawa, H. Kawai, K. Ando, K. Takanashi, S. Maekawa, and E. Saitoh, *Nature* **464**, 262 (2010).
- <sup>8</sup>A. A. Serga, A. V. Chumak, and B. Hillebrands, *J. Phys. D: Appl. Phys.* **43**, 264002 (2010).
- <sup>9</sup>N. Adachi, V. P. Denysenkov, S. I. Khartsev, A. M. Grishin, and T. Okuda, *J. Appl. Phys.* **88**, 2734 (2000).
- <sup>10</sup>Landolt-Börnstein, *Numerical Data and Functional Relationships in Science and Technology*, New Series, Group III, Vol. 27/e (Springer-Verlag, Berlin, 1991).
- <sup>11</sup>Z. C. Xu, M. Yan, M. Li, Z. L. Zhang, and M. Huang, *J. Appl. Phys.* **101**, 053910 (2007).
- <sup>12</sup>S. Tsunashima, *J. Phys. D: Appl. Phys.* **34**, R87 (2001).
- <sup>13</sup>S. A. Manuilov, R. Fors, S. I. Khartsev, and A. M. Grishin, *J. Appl. Phys.* **105**, 033917 (2009).
- <sup>14</sup>S. Wittekoek, T. J. A. Popma, J. M. Robertson, and R. F. Bongers, *Phys. Rev. B* **12**, 2777 (1975).
- <sup>15</sup>P. Hansen and J.-P. Krumme, *Thin Solid Films* **114**, 69 (1984).
- <sup>16</sup>M. Deb, E. Popova, A. Fouchet, and N. Keller, *J. Phys. D: Appl. Phys.* **45**, 455001 (2012).
- <sup>17</sup>A. Mekonnen, M. Cormier, A. V. Kimel, A. Kirilyuk, A. Hrabec, L. Ranno, and Th. Rasing, *Phys. Rev. Lett.* **107**, 117202 (2011).
- <sup>18</sup>J. Kaplan and C. Kittel, *J. Chem. Phys.* **21**, 760 (1953).
- <sup>19</sup>A. H. M. Reid, A. V. Kimel, A. Kirilyuk, J. F. Gregg, and Th. Rasing, *Phys. Rev. Lett.* **105**, 107402 (2010).
- <sup>20</sup>S. Serrano-Guisan, K. Rott, G. Reiss, and H. W. Schumacher, *J. Phys. D* **41**, 164015 (2008).
- <sup>21</sup>O. Büttner, M. Bauer, C. Mathieu, S. O. Demokritov, B. Hillebrands, P. A. Kolodin, M. P. Kostylev, S. Sure, H. Dötsch, V. V. Grimalsky, Yu. Rapoport, and A. N. Slavin, *IEEE Trans. Magn.* **34**, 1381 (1998).
- <sup>22</sup>M. J. Hurben and C. E. Patton, *J. Magn. Magn. Mater.* **163**, 39 (1996).